

BID: Boundary-Interior Decoding for Unsupervised Temporal Action Localization Pre-Training

Qihang Fang¹ Chengcheng Tang² Shugao Ma² Yanchao Yang¹

Abstract

Skeleton-based motion representations are robust for action localization and understanding for their invariance to perspective, lighting, and occlusion, compared with images. Yet, they are often ambiguous and incomplete when taken out of context, even for human annotators. As infants discern gestures before associating them with words, actions can be conceptualized before being grounded with labels. Therefore, we propose the first unsupervised pre-training framework, *Boundary-Interior Decoding (BID)*, that partitions a skeleton-based motion sequence into discovered semantically meaningful *pre-action* segments. By fine-tuning our pre-training network with a small number of annotated data, we show results out-performing SOTA methods by a large margin.

1. Introduction

Developing a human-centric AI assistant providing timely assistance and feedback, as a collaborator for constructing a project or an instructor for learning a skill, requires a system that thoroughly understands human actions. A premise to action understanding is the ability to recognize and segment human actions from a long sequence, through the temporal action localization (TAL) task, which is critical as a standalone application and foundational for downstream tasks such as alignment and detailed action recognition.

Model pre-training, which involves learning representations from large-scale data, has become a common practice for vision-based temporal action classification. This approach has proven to be effective for temporal action classification (TAC) (Carreira & Zisserman, 2017; Wang et al., 2016), which aims to predict video-level or instance-level action

¹The University of Hong Kong ²Meta Reality Labs. Correspondence to: Chengcheng Tang <chengcheng.tang@meta.com>, Yanchao Yang <yanchao.yang@hku.hk>.

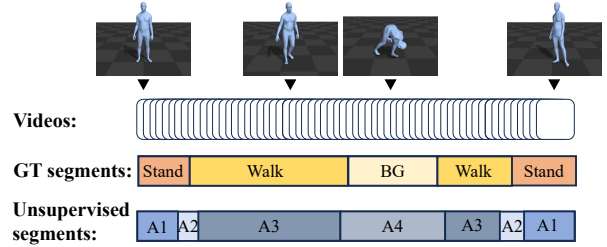


Figure 1. We propose an unsupervised method to partition a skeletal motion to semantically meaningful action segments, which we name as *pre-action* segments and classes to differentiate from those defined by human annotators. We study how the discovery of pre-actions can help improve label efficiency with fine-tuning on limited human labels, for temporal action localization.

labels for trimmed data. However, TAC disregards the start time and duration of each action, which are crucial for temporal action localization (TAL). As a result, the pre-training features derived from TAC are insufficient for TAL, which needs to infer the start time and duration for each action with untrimmed sequences. In recent years, some researchers (Alwassel et al., 2021; Xu et al., 2021a;b) begin to address this issue by developing specific methods for TAL tasks. However, these methods heavily rely on large-scale annotated video data, which is challenging and expensive to annotate accurately with untrimmed videos, particularly when facing a large range of ambiguous action types. (Zhang et al., 2022) proposed the first unsupervised pre-training method for vision-based TAL. Their approach involves designing a contrast learning task disentangling interleaved videos from different sequences through data augmentation. However, inserting and rediscovering artificially cut clips from one video into another without semantics disrupts the continuity of the action sequence. As a result, this approach faces challenges in locating accurate segmentation boundaries.

While vision-based temporal action localization (TAL) has made significant progress, it has limitations in terms of robustness towards viewpoints, lighting conditions, and image noise. In contrast, 3D skeleton-based data provides a more reliable representation for applications such as animation, augmented reality, and gaming. As a result, there is a growing interest in action understanding for skeleton-based data

(Punnakkal et al., 2021; Yu & Fujiwara, 2023). At the same time, skeleton-based tasks require a specific focus on human posture during actions due to the absence of visual context. For instance, vision-based tasks can determine if an athlete is playing basketball based on the presence of a basketball court, whereas such contextual information is not available for skeleton-based tasks. Due to the unique challenges, most existing skeleton-based methods (Punnakkal et al., 2021; Vemulapalli et al., 2014; Du et al., 2015) primarily focus on TAC instead of TAL. Recently, (Yu & Fujiwara, 2023) proposed the first skeleton-based TAL algorithm that incorporates a weakly supervised pre-training step using sequence-level annotation available to the input untrimmed videos. However, as the sequence-level annotation often lacks granularity and temporal resolution, the pre-training results are susceptible to long-tail effects, facing challenges in capturing shorter and infrequent actions.

To address the issues mentioned above, we propose *BID* which is an unsupervised pre-training method for skeleton-based temporal action localization. We regard human actions as different flow fields and train a decoding function to represent these flow fields by discrete latent codes. Through these flow fields, we can discover meaningful action segmentation and classification without human annotation. To achieve this, we enforce that the discrete latent codes inform the states within each action segment, for which we train an *Interior Decoder* that can inpaint the random masked sequence based on the latent codes. Besides, we also require the discrete latent codes to inform or help select the end state of the action, for which we instantiate a *Boundary Decoder* to predict the end state for each action segment. By supervising these two decoders, we can achieve semantically meaningful segmentation and classification. Once we obtain the discrete action representations of human motion, we can employ them for Temporal Action Localization (TAL) with fine-tuning on a limited number of annotations.

To evaluate the effectiveness of our proposed method for TAL, we conduct experiments using the BABEL dataset (Punnakkal et al., 2021) and compared it with another skeleton-based method (Yu & Fujiwara, 2023) and other vision-based methods (Zhang et al., 2022; 2021; Huang et al., 2021; Rajasegaran et al., 2023) adapted to the skeleton-based settings. We show that our method outperforms existing methods, indicating the semantic meaningfulness and groundability of pre-action segments and classes emerged through our proposed method of unsupervised skeleton-based temporal action localization.

We summarize the contributions of this paper as follows:

- We introduce *BID*, which, to our best knowledge, the first unsupervised skeleton-based method for temporal action localization through a pre-training framework.
- By modeling actions as bounded and directed flow fields,

we propose two optimization targets for the pre-training framework, focusing on the interior and boundary of segments respectively.

- We conduct comprehensive evaluations and comparisons of our approach, outperforming SOTA methods by 20%. We study emerged pre-action classes and segments qualitatively, quantitatively, and visually, validating that, without any human annotation, the proposed pre-training framework develops a surprisingly strong sense of semantic understanding that correlates with human annotated action class labels and segments.

2. Related Work

Unsupervised Representation Learning. In the recent era, computer vision rediscovered the power of unsupervised learning (Caron et al., 2020; Chen et al., 2020a; Chen & He, 2020; Chen et al., 2020b; Grill et al., 2020; He et al., 2020; Wu et al., 2018).

In (Qian et al., 2021), the authors propose a novel framework that leverages the temporal dynamics and spatial features in videos to learn rich, discriminative representations. In (Wang et al., 2020), the authors introduce a self-supervised learning approach for video representation that is based on predicting the pace of video sequences, training a model to distinguish between normal and temporally altered (e.g., sped-up or slowed down) video clips. In (Yang et al., 2020), the authors propose a technique that aligns the representations of video segments with varying tempos, ensuring that the learned representations are consistent across different speeds of motion. In different contexts, contrastive learning with videos has shown promise for a wide range of vision-based tasks. For example, employing positive-augmented contrastive learning to better distinguish between closely related captions and visual content enhances image and video captioning evaluation (Sarto et al., 2023); a semi-supervised contrastive learning framework for ego-vehicle action recognition also improves the accuracy and robustness of action recognition in autonomous driving scenarios (Noguchi & Tanizawa, 2023).

Temporal Action Classification. Temporal action classification (TAC) is also known as action recognition, which aims to predict sequence-level or video-level action labels for trimmed data. Earlier works on action recognition rely on handcrafted features (Vemulapalli et al., 2014; Liu et al., 2016; Dollár et al., 2005; Wang & Schmid, 2013). Among the tasks of video and action understanding, TAC of trimmed data or vision-based action recognition (Shi et al., 2019; Feichtenhofer et al., 2019; Rajasegaran et al., 2023) is a popular task. At first, 3D convolution networks are the commonly adapted backbone for vision-based understanding (Taylor et al., 2010; Tran et al., 2015). Considering that 3D

convolution networks treat the spatial and temporal information similarly, optical flow (Shi et al., 2019) is introduced in this field. SlowFast (Feichtenhofer et al., 2019) utilizes video streams but at different frame rates to learn to fuse spatial and temporal information. Besides, Another line of works (Pan et al., 2021; Wang et al., 2018; Wang & Gupta, 2018) focuses on the relationship between actors and objects rather than the model structure.

For skeleton-based action recognition, some work (Du et al., 2015; Liu et al., 2016) utilizes the RNN-based method to extract the temporal information from the human joint sequences. CNN-based methods (Liu et al., 2017; Ke et al., 2017) are also introduced in this task. Furthermore, ST-GCN (Yan et al., 2018) proposes to model the skeleton-based data to graph structure which can be cooperated with ST-GCN, which utilizes the connectivity of human joints. Adaptive graph convolutional network (AGCN) (Shi et al., 2019) extends ST-GCN by parameterizing the graph structure of skeleton data and embedding it into the network. Recently, unsupervised methods for action recognition based on ST-GCN have been developed, such as AimCLR (Guo et al., 2022) and ActCLR (Lin et al., 2023). These methods aim to learn representations without relying on annotated labels.

Temporal Action Localization (TAL) Task. Unlike action recognition task (Carreira & Zisserman, 2017; Feichtenhofer et al., 2019; Lin et al., 2019a; Tu et al., 2019; Wang et al., 2016), the target of TAL is to temporally localize the action of interest in untrimmed videos. In general, TAL tasks can be split into two different sub-tasks, temporal action segmentation and temporal action classification. Some previous methods utilize temporal anchor to compose action window (Buch et al., 2017; Heilbron et al., 2016; Lin et al., 2017). Some other works segment the actions by directly predicting the boundary probabilities (Lin et al., 2019b). Furthermore, the combination of segmentation and classification is also explored (Lin et al., 2019b; Xu et al., 2017; 2020).

Due to the dataset scale and GPU memory constraints, some works (Alwassel et al., 2021; Xu et al., 2021a;b) tackle pre-train models on large-scale trimmed TAC datasets and then use it to extract frame-level or segment-level features in untrimmed TAL data. Motivated by the recent success of unsupervised learning, the approach by (Zhang et al., 2022) introduces a novel method for segmenting actions using unsupervised learning. They introduce a novel self-supervised pretext task called Pseudo Action Localization (PAL). Subsequently, in (Yu & Fujiwara, 2023), the authors proposed a novel problem of skeleton-based weakly-supervised temporal action localization (S-WTAL), recognizing and localizing human action segments in untrimmed skeleton videos given only the video-level labels.

3. Problem Statement

3.1. Skeleton-Based Temporal Action Localization

Give a skeleton-based untrimmed motion sequence $S = \{s_i\}_{i=1}^T \in \mathbb{R}^{T \times J}$, where T is the number of frames for the temporal sequence and J is the total number of degrees of freedom of skeletal joints, the goal of the temporal action localization (TAL) task is to divide the sequence to mutually exclusive segments with action labels, $\{t_m^b, t_m^e, a_m\}_{m=1}^M$, where t_m^b, t_m^e, a_m are the beginning, end timestamps and action class of the m -th predicted action.

Traditionally, the action labels are predefined and manually labeled in a dataset. In this work, we study a new problem where the action labels are not available, and we propose a unsupervised method to discover semantically meaningful actions (or segments of a motion trajectory), which we name as *pre-action* segments and classes to differentiate from those defined by human annotators. We will then study how the discovery of pre-actions can help improve label efficiency with fine-tuning on limited human labels.

3.2. Action Flow Field

From the Lagrangian point of view, the motion of an object moving in space can be represented as a flow field, i.e., a function that describes the relationship between time and the object’s position:

$$x_t = \mathcal{G}(t), \quad (1)$$

where $\mathcal{G}(\cdot)$ is the flow that characterizes the position of the object x_t at time t in a reference coordinate frame.

Human motion sequences can be similarly represented as a flow field of human bodies moving through space and time (Rajasegaran et al., 2023), with different actions represented by distinctive flow fields. Thus, we utilize the concept of flow fields in Equation 1 to represent human actions, and reformulate it in the context of skeleton-based TAL:

$$s_t = \mathcal{G}^{a_m}(t), t_m^b \leq t \leq t_m^e, \quad (2)$$

where \mathcal{G}^{a_m} is the flow field characterizing action a_m and s_t is the motion frame at the timestamp t . We call the flow field representing human actions the *action flow field*.

4. Unsupervised TAL Pre-Training

We aim to build an unsupervised skeleton-based pre-training framework that divides an input motion sequence into semantically meaningful segments with action features categorizing action flow fields without annotation.

Specifically, we train a neural motion encoding function, \mathcal{E} , unsupervised, to partition the input sequence S to multiple segments $\{p_m\}_{m=1}^M$ with $p_m = \{s_t\}, t = t_m^b \dots t_m^e$, whose

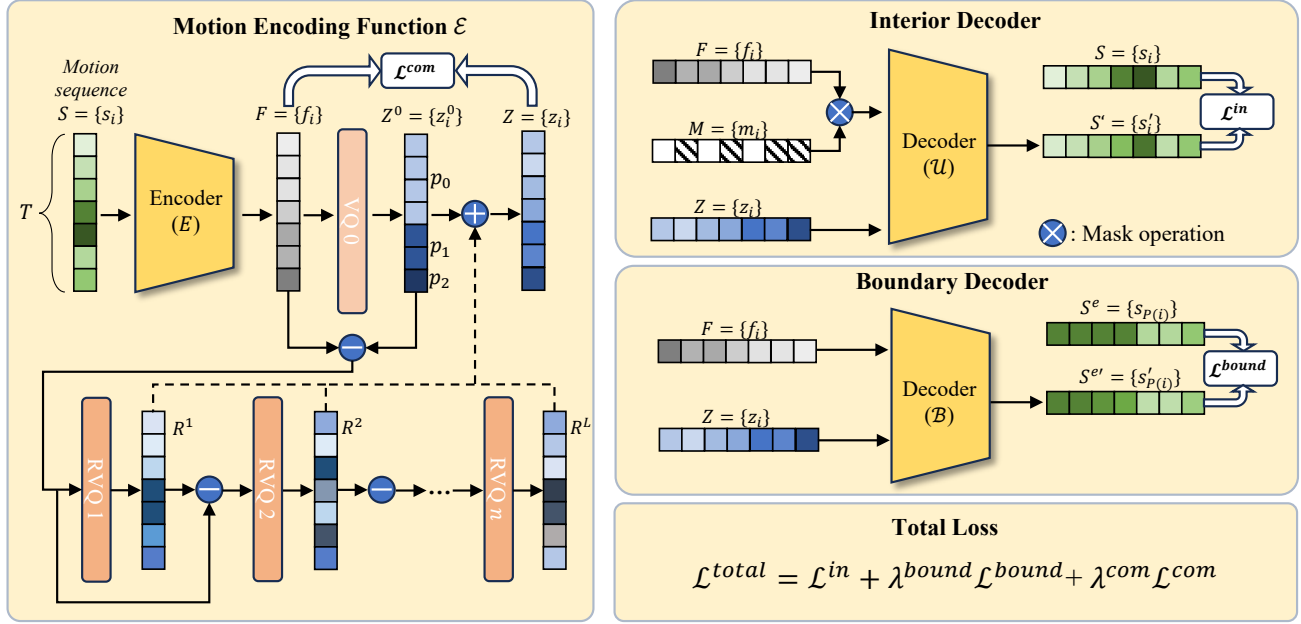


Figure 2. An overview of the proposed framework, which consists of a motion encoding function \mathcal{E} , an interior decoder \mathcal{U} , and a boundary decoder \mathcal{B} . The motion encoding function \mathcal{E} is composed of a linear encoder E and a residual VQ (RVQ) module, which encodes the input motion sequence S into discrete latent codes. The frames with the same discrete latent code predicted by the VQ layer are considered with the same action class. The summation of the discrete latent codes from the VQ layer and the RVQ layers is used as the class representation of the motion frames. Besides the commitment loss for training the RVQ module, we devise two optimization objectives that encourage the class representation to be informative about the state transition within an action and the ending state of that action.

action label is a_m . The number of action classes N is predefined and equal to the maximum possible number of action classes in the dataset. Due to the lack of ground-truth labels, these segments and actions may not be completely aligned with human annotations. And as mentioned above, we call these segments, $\{p_m\}_{m=1}^M$, *pre-action segments* or actions, $\{a_m\}_{m=1}^M$, *pre-action classes*.

To enable training, we propose that the *pre-action class* a_m should help instantiate a flow field function \mathcal{G}^{a_m} that can be used to reconstruct or predict the temporal movements of the human body within this action clip. Through learning for these flow field functions, we can discover meaningful *pre-action segments* and *pre-action classes*. More explicitly, we enforce that the pre-action class should inform the states within each action clip as much as possible, for which we train an *Interior Decoder* that reconstructs the state transitions within the segment from the masked clip and the discovered class representation. Moreover, the discovered action class should inform or help select the end state of the action, for which we instantiate a *Boundary Decoder* that predicts the terminating state $s_{t_m}^e$ from the current state and the class. An overview of the training scheme is shown in Figure 2. Once we obtain the discrete action representations of human motion, we can employ them for Temporal Action Localization (TAL) with fine-tuning on a limited number of annotations. Next, we detail the neural architecture for

learning the encoding function \mathcal{E} .

4.1. Motion Encoding Function

Vector Quantized Variational AutoEncoder (VQ-VAE) (Van Den Oord et al., 2017) are widely used to represent human motion as discrete latent codes (Van Den Oord et al., 2017; Zhang et al., 2023; Jiang et al., 2023) in the literature of motion generation and synthesis. We also leverage VQ-VAE to construct the temporal-spatial encoding function \mathcal{E} for extracting discrete latent codes to represent different actions. The VQ-VAE-based encoding function \mathcal{E} is composed of a linear encoder E and a VQ layer. The VQ layer contains a codebook c to quantize the input continuous features into discrete latent codes. Specifically, E encodes the input sequence S into a sequence of features $F \in \mathbb{R}^{T \times D}$, with T per-frame features $\{f_i\}_{i=1}^T$, where $f_i \in \mathbb{R}^D$:

$$F = E(S), \text{ where } F \in \mathbb{R}^{T \times D}. \quad (3)$$

The codebook $c \in \mathbb{R}^{K \times D}$ represents different action flow fields, where K is a predefined number of different discrete codes or motion modes and $c_k \in \mathbb{R}^D$ is the k -th action representation. The VQ layer encodes the sequence feature F to a discrete latent code(s) $Z \in \mathbb{R}^{T \times D}$ through codebook c by projecting each per-frame feature f_i to its nearest code:

$$VQ(f_i) = c_k, \text{ where } k = \operatorname{argmin}_j \|f_i - c_j\|_2^2, \quad (4)$$

where VQ represents the VQ layer, Z is the ensemble $\{VQ(f_i)\}_{i=1}^T$, and k is the code index corresponding to a *pre-action class*. We consider adjacent motion frames assigned with the same *pre-action class* constituting a *pre-action segment*. To facilitate learning and guarantee convergence, we impose a commitment loss following (Van Den Oord et al., 2017):

$$\mathcal{L}^{com} = \sum_{i=1}^T \|f_i - sg(VQ(f_i))\|_2^2, \quad (5)$$

where sg is the stop-gradient operation.

4.2. Residual VQ-VAE

In practice, we find two problems with the VQ-VAE-based encoding: 1) Codebook collapse, where only a small number of codes in the codebook are activated, and a large number of codes are rarely used; 2) Imbalance of high-frequency information and action semantics. To retain enough high-frequency information for good reconstruction quality, one could increase the number of codes in the codebook to avoid over-compress. However, increasing the number of discrete latent codes will make the *pre-action segments* become over-fragmented and semantically ambiguous.

Similar phenomena are also reported in motion generation (Yao et al., 2023), audio compression (Zeghidour et al., 2021), and image generation (Lee et al., 2022). To solve these problems, Residual VQ-VAE (Lee et al., 2022) has been proposed, which employs a residual architecture with multiple quantization layers to enhance the utilization of the codebook and stabilize the training process. In addition to the standard VQ-VAE, we also employ a series of residual vector quantization (RVQ) layers to resolve the above issues (Figure 2). More explicitly, we first utilize the VQ layer to quantize input feature F to discrete latent code Z^0 . Then, an RVQ layer is utilized to quantize the residual $F - Z^0$ to discrete latent code R^1 . Subsequent, the l -th RVQ layer is utilized to quantize the residual $F - Z^0 - \sum_{i=1}^{l-1} R^i$ to discrete latent code R^l . With the RVQ layers, the final quantized code Z for input F is the sum of all the discrete code,

$$Z = Z^0 + \sum_{l=1}^L R^l, \quad (6)$$

where L is the number of RVQ layers.

In (Lee et al., 2022), the VQ layer and all the RVQ layers share the same codebook to increase the usage of the codebook. However, repeatedly extracting discrete codes from the same codebook makes it difficult to define the *pre-action classes*. Considering that the Residual VQ-VAE builds a coarse-to-fine representation of the entire latent

space (Yao et al., 2023; Lee et al., 2022), we initialize two different codebooks c^{VQ} and c^{RVQ} for the VQ layer and RVQ layers respectively. The first codebook is only used for the VQ layer, while the frames with the same discrete code quantized by the VQ layer are considered with the same *pre-action class*. The second codebook is shared by all the RVQ layers for retaining details important for reconstruction but not high-level semantics.

4.3. Boundary and Interior Decoding for Pre-Actions

To partition an input motion sequence to semantically meaningful *pre-action* segments and classes, we optimize the discrete latent codes representing the action flow fields for the informativeness of both the state transitions within an action (Interior Decoding) and the ending state of that action (Boundary Decoding).

Interior Decoding. Given an untrimmed motion sequence S with several *pre-action segments* $p_m = \{t_m^b, t_m^e, a_m\}$ (abuse notation for simplicity), the motion frames $\{s_i\}_{i=t_m^b}^{t_m^e}$ belonging to a *pre-action segment* p_m can be regarded as state transitions in the interior of the segment governed by the action flow field defined by a_m . Thus, we propose that the action flow field generated from the discrete latent codes $\{z_i\}_{i=t_m^b}^{t_m^e}$ (action representation) should be as close as possible to the input states $\{s_i\}_{i=t_m^b}^{t_m^e}$.

A naive approach to achieving this optimization goal is to directly reconstruct the sequence S . However, in practice, we find that this method results in scattered *pre-action segments* of short lengths with poor semantic meaning. Therefore, we propose to achieve this objective through inpainting, by instantiating an interior decoder \mathcal{U} that predicts the full state sequence from a randomly masked one and the class representation. Specifically, we apply a random mask $M \in \mathbb{R}^T$ to the sequence feature F encoded by the linear encoder E , which is subsequently concatenated with the discrete latent code Z as the input for the interior decoder, \mathcal{U} . The reason we use sequence features F instead of the original motion frames S as input is to ensure that gradients can be propagated to the encoder E . The output of the interior decoder \mathcal{U} is the completed motion sequence $S' = \{s'_i\}_{i=1}^T$. We apply the L2-norm to optimize this discrepancy,

$$\mathcal{L}^{in} = \|\mathcal{U}(F \circ M, Z) - S\|_2^2, \quad (7)$$

where \circ indicates the masking operation.

Boundary Decoding. To further improve the semantic meaningfulness of the discovered action classes, we ask that the discrete action representations be informative about the ending states when an action is completed. Also, given a segment p_m , its final frame $s_{t_m^e}$ is indicative of human switching from one action to another. Thus, an action representation can be of more semantic significance if it can help

distinguish a boundary (action-switching) state from others.

To achieve this goal, we initialize a boundary decoder, \mathcal{B} , to predict the boundary states. Similar to the interior decoder, \mathcal{U} , the boundary decoder, \mathcal{B} , takes the sequence feature, F , and the discrete latent code, Z , as input, and predict the end-of-segment frame poses, $S^e = \{s_{P(i)}\}_{i=1}^T$, where $P(i)$ is the boundary frame timestamp t_m^e of predicted *pre-action segment* p_m that contains frame s_i . Note that $S^e \in \mathbb{R}^{T \times J}$ has the same dimension as S , which are constructed by repeating the predicted boundary poses from the input sequence S , i.e., all frames in an action segment are populated with the boundary one. And we also apply the L2-norm to optimize the boundary decoder:

$$\mathcal{L}^{bound} = \|\mathcal{B}(F, Z) - S^e\|_2^2. \quad (8)$$

The **total training loss** \mathcal{L}^{total} for our unsupervised temporal action location pre-training is summarized as:

$$\mathcal{L}^{total} = \mathcal{L}^{in} + \lambda^{bound} \mathcal{L}^{bound} + \lambda^{com} \mathcal{L}^{com}, \quad (9)$$

where λ^{bound} and λ^{com} are predefined weights and studied in the experiments.

5. Experiments

5.1. Experiment Setup

To evaluate our proposed method, we pre-train and transfer our model as follows: We first pre-train the whole network on a large-scale untrimmed skeleton-based dataset without annotation. Then, we finetune the network on an annotated dataset by adding a linear classifier (a residual block (He et al., 2016) followed by a softmax layer) after the pre-trained linear encoder E without the decoders \mathcal{U} and \mathcal{B} .

Datasets. We verify our method on the benchmark dataset, BABEL (Punnakkal et al., 2021). Most of the temporal action localization datasets are vision-based. To the best of our knowledge, BABEL is the only 3D human motion dataset with frame-level action annotation, which contains about 43 hours of motion sequences and over 250 action categories from AMASS (Mahmood et al., 2019). We follow S-WTAL (Yu & Fujiwara, 2023) that create 3 subsets of BABEL, each of which consists of 4 action categories. We pre-train our model on all of the 3 subsets and apply fine-tuning for the subsets separately.

Implementation details. We utilize a Temporal Convolutional Network (TCN) structure for both the encoder and decoders. Our model is trained using the Adam optimizer with an initial learning rate of 10^{-3} . This rate undergoes a warm-up over the first 20 epochs and is then reduced to one-tenth of its value at the 20th and the 40th epochs. The training spans 500 epochs for both pre-training and fine-tuning phases. We utilize a batch size of 128, and the

Table 1. Temporal action localization performance comparisons over BABEL. The column Avg indicates the average mAP at IoU thresholds from 0.1 to 0.5.

Subset-1						
Method	Detection mAP @ IoU (%)					Avg
	0.1	0.2	0.3	0.4	0.5	
CoLA	27.40	14.63	6.43	4.03	2.15	10.93
FAC-Net	29.65	17.65	8.48	3.88	2.62	12.46
LART	52.34	45.81	38.62	30.15	23.82	38.15
S-WTAL	48.74	39.82	33.15	27.39	21.70	34.16
UP-TAL	54.83	49.72	43.70	38.05	32.37	43.73
Ours	59.57	53.47	46.90	41.00	35.01	47.20
Subset-2						
Method	Detection mAP @ IoU (%)					Avg
	0.1	0.2	0.3	0.4	0.5	
CoLA	40.10	26.86	19.9	14.02	10.32	22.24
FAC-Net	34.18	19.84	12.95	9.03	6.53	16.51
LART	47.74	33.47	25.90	18.98	15.43	28.30
S-WTAL	61.01	50.26	40.36	29.84	19.55	40.20
UP-TAL	62.10	57.55	49.17	41.16	30.49	48.09
Ours	64.81	61.05	53.39	42.98	35.13	51.47
Subset-3						
Method	Detection mAP @ IoU (%)					Avg
	0.1	0.2	0.3	0.4	0.5	
CoLA	21.50	17.40	15.16	12.10	8.99	15.03
FAC-Net	27.51	22.26	17.64	14.05	8.90	18.07
LART	40.67	32.25	24.56	20.03	16.38	26.78
S-WTAL	35.81	31.45	26.55	23.42	20.36	27.52
UP-TAL	40.20	37.15	31.94	26.85	25.19	32.27
Ours	42.81	37.96	33.54	29.47	24.60	33.68

training is executed on a single NVIDIA Tesla A100 GPU. We set T , J , N , λ^{bound} and λ^{com} as 120, 75, 64, 1.0, and 0.05, respectively, by default.

Comparison baselines. We compare our method with S-WTAL (Yu & Fujiwara, 2023), a weakly-supervised skeleton-based temporal activity localization method. Recognizing the predominance of vision-based methods in this field, we adapt vision-based methods CoLA (Zhang et al., 2021), FAC-Net (Huang et al., 2021), and LART (Rajasegaran et al., 2023) to skeleton-based settings for comparison. CoLA and FAC-Net are both weakly-supervised vision-based TAL algorithms, and LART is the SOTA fully-supervised vision-based TAL method. We also adapt UP-TAL (Zhang et al., 2022) which is a vision-based unsupervised approach for temporal action localization pre-training.

Evaluation metrics. We follow the standard evaluation protocol. We calculate the Mean Average Precisions (mAPs) under different temporal Intersection of Union (IoU) thresholds, by segmenting sequences based on the frame-level prediction following FAC-Net (Huang et al., 2021).

5.2. Quantitative Analysis

We show the mAP of the detected action segments on the three subsets in Table 1. Addressing the complexities of

Table 2. Results of analysis for different action categories.

Method	Detection mAP @ IoU (%)											
	Walk	Stand	Turn	Jump	Sit	Run	Stand up	Kick	Jog	Wave	Dance	Gesture
CoLA	43.87	37.98	14.68	13.07	78.40	40.35	19.20	22.45	23.03	5.93	43.67	13.36
FAC-Net	49.17	31.65	22.52	15.24	57.11	36.59	16.44	26.57	40.45	15.28	42.56	11.76
LART	74.57	65.78	41.04	27.97	85.70	33.13	<u>43.07</u>	29.07	52.36	<u>25.54</u>	61.91	22.94
S-WTAL	79.37	74.32	24.28	17.03	<u>83.74</u>	57.49	23.59	<u>79.21</u>	45.45	16.93	66.13	14.75
UP-TAL	<u>79.93</u>	70.15	33.44	<u>35.77</u>	81.83	51.21	46.45	<u>68.92</u>	<u>59.29</u>	29.04	50.06	22.42
Ours	81.86	<u>71.81</u>	<u>38.87</u>	45.71	77.10	<u>54.86</u>	48.00	79.28	61.52	21.20	<u>65.91</u>	<u>22.79</u>

skeleton-based temporal action localization, our approach aligns with the benchmark set by S-WTAL (Yu & Fujiwara, 2023), evaluating mAP at thresholds ranging from 0.1 to 0.5, along with their average. In our experiments, our method consistently outperforms other baseline approaches.

CoLA (Zhang et al., 2021) and FAC-Net (Huang et al., 2021) are designed for weakly-supervised vision-based tasks. Thus, extracting the necessary information from visual elements is a key factor in their design. Simply altering the feature extractor of these methods to fit the skeleton-based task leads to poor performance. LART (Rajasegaran et al., 2023) is a fully supervised method that combines the skeleton and visual information for TAL. The absence of vision-based data also impacts the performance of LART on our test set. S-WTAL (Yu & Fujiwara, 2023) utilizes sequence-level labels to learn the TAL method. Considering that the sequence-level features are mainly influenced by the high-frequency and long actions, it encounters serious long-tail effect. Thus, S-WTAL works worse than UP-TAL and our method, which exploits the frame-level feature for pre-training. Although UP-TAL (Zhang et al., 2022) is also vision-based, it not only focuses on visual context but also emphasizes the continuity of action frames, making it more effective for skeleton-based tasks, thus outshining other vision-based methods.

Moreover, we detail the mAP at a threshold of 0.1 for different action classes in 2. Considering the diverse duration and quantities of different action categories in the dataset, it is crucial to address the issue of balancing different action categories during the training process and mitigate the long-tail effect. S-WTAL, which relies on sequence-level annotation for training, is notably susceptible to this variation in class distribution. In contrast, our method of unsupervised pre-training adeptly captures the intrinsic structure of raw data, mitigating the long-tail effect induced by data distribution. Further, our approach surpasses UP-TAL because we learn the segmentation and classification based on the original sequence rather than discontinuous pasted sequences. This enables our network to acquire features tailored to action classes with fewer samples while maintaining robust performance across more prevalent categories.

Validation for the number of action discrete codes. We

further evaluate the influence of the number of *pre-action classes* for VQ layer. Too few classes prevent the network from distinguishing different actions during pre-training, but too many codes cause the distinguished actions to be too short, and lacking in semantics. The work related to human motion reconstruction (Jiang et al., 2023; Zhang et al., 2023) typically uses more than 128 codes, allowing for a detailed description of motion within a few adjacent frames. However, for our task, we are focused on actions within a longer time window, and intuitively, we need fewer code numbers.

We test five different settings of pre-action class numbers K : 16, 32, 64, 128, and 256 on three subsets of BABLE (Punnakkal et al., 2021) and their union set, as shown in table 5. We observe that for these subsets, choosing $K = 64$ is shown to be more effective for most settings. Too much or too little code can lead to a decrease in algorithm performance.

Table 3. Numerical results on the different number of pre-action classes.

Subset-1						
Method	Detection mAP @ IoU (%)					Avg
	0.1	0.2	0.3	0.4	0.5	
$K = 16$	56.54	<u>53.12</u>	48.17	42.88	36.95	47.53
$K = 32$	56.99	51.91	46.34	40.63	34.05	45.99
$K = 64$	59.57	53.47	46.90	41.00	<u>35.01</u>	<u>47.20</u>
$K = 128$	<u>58.36</u>	53.09	<u>47.60</u>	<u>41.48</u>	34.28	46.96
$K = 256$	57.10	52.24	46.80	40.71	34.09	46.19
Subset-2						
Method	Detection mAP @ IoU (%)					Avg
	0.1	0.2	0.3	0.4	0.5	
$K = 16$	60.71	55.24	48.12	42.04	33.63	47.95
$K = 32$	62.82	57.98	<u>52.42</u>	43.64	<u>35.44</u>	<u>50.86</u>
$K = 64$	64.81	61.05	53.39	42.98	35.13	51.47
$K = 128$	<u>63.67</u>	<u>59.31</u>	50.87	43.28	35.58	50.54
$K = 256$	61.31	58.37	49.28	40.36	32.99	48.46
Subset-3						
Method	Detection mAP @ IoU (%)					Avg
	0.1	0.2	0.3	0.4	0.5	
$K = 16$	40.02	35.49	28.80	24.32	20.04	29.73
$K = 32$	43.48	36.68	<u>28.95</u>	<u>26.92</u>	23.71	<u>31.95</u>
$K = 64$	<u>42.81</u>	37.96	33.54	29.47	24.60	33.68
$K = 128$	37.38	32.74	26.07	22.61	19.31	27.62
$K = 256$	41.23	<u>37.03</u>	28.65	25.47	20.96	30.67

Ablation study. To further validate the design of our algorithm, we have designed the following ablation study:

- **Ours - w/o RVQ:** We remove the RVQ layers and utilize Z^0 as the output discrete latent code to validate the benefits of Residual VQ-VAE.
- **Ours - w/o M :** We remove the mask operation for the input of \mathcal{U} . In this way, we modify the sequence inpainting task into a reconstruction task.
- **Ours - w/o \mathcal{U} :** We delete the interior decoder \mathcal{U} and loss \mathcal{L}^{in} to validate the benefits of interior constraint.
- **Ours - w/o \mathcal{B} :** We delete the boundary decoder \mathcal{B} and loss \mathcal{L}^{bound} to validate the benefits of boundary constraint.

The results are demonstrated in Table 4. The complete version of our algorithm outperforms the modified versions across different subsets. When we modify the sequence inpainting task into a reconstruction task by removing the mask operation for \mathcal{U} , the performance decreases on all subsets, and it even is weaker than the version where only \mathcal{B} is retained, which demonstrate that reconstruction-based optimization objectives reduce the network’s ability to segment and classify different action categories. This is because the reconstruction process leads to shorter *pre-action segments* with less semantic clarity, which is not suitable for TAL task. Besides, the imbalance of detail information and action semantics and the problem of codebook collapse caused by a single code book, make the network without RVQ layers of the network significantly weaker than other settings in Sets 1 and 3. Meanwhile, both optimization objectives are beneficial to the results, and the removal of any one of them leads to a decline in the performance of the algorithm. These experiments indicate that each key component of our algorithm design contributes to its enhancement.

Table 4. Numerical results for ablation study
Average detection mAP @ IoU (%)

Method	Detection mAP @ IoU (%)		
Ours - recon	46.63	48.74	31.22
Ours - w/o RVQ	45.29	50.55	27.58
Ours - w/o \mathcal{U}	46.82	48.72	31.43
Ours - w/o \mathcal{B}	46.97	49.15	31.19
Ours	47.20	51.47	33.68

Confusion matrix for our prediction and ground truth action classes. To further identify the current bottlenecks of our algorithm, we conduct evaluation on the union set of these three subsets, including 12 action classes. Additionally, we compute a confusion matrix comparing the predicted action classes to the ground truth as shown in Figure 3 which reveals that the primary factor impacting our algorithm’s performance is the background, apart from the targeted 12 action categories. The impact of background is twofold. Firstly, the background occupies a significant portion of the entire sequence and contains a high level of diversity, making its segmentation more challenging compared to other categories. Secondly, different action classes may exhibit similar motion frames. For instance, in BA-

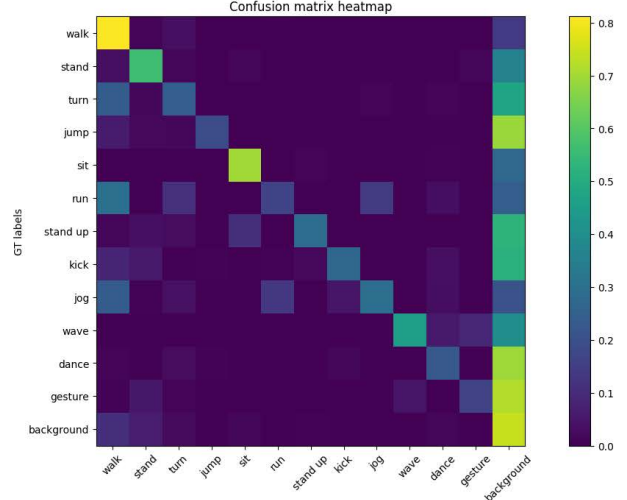


Figure 3. We calculate the confusion matrix comparing the predicted action classes to the ground truth to identify the bottlenecks of our method. We conduct evaluation on the union set of the three subsets, including 12 action classes.

BEL, the classes “step” and “move back to original position” visually resemble “walk”. However, “step” and “move back to original position” are listed in the background, which introduces label noises for background segmentation.

6. Conclusion

We propose a novel unsupervised pre-training method for skeleton-based temporal action localization. We consider different actions as different flow fields and represent these flow fields as discrete latent codes. To make these flow fields semantically meaningful, we design two optimization objectives to encourage these discrete latent codes to be informative about the state transition within an action and the ending state of that action. Further, we demonstrate the benefits of the latent space learned through our method for temporal action localization, both through comparison with the baselines and through ablation experiments.

However, our approach is still limited in some aspects.

- When the motion data exhibits significant diversity in the background, our algorithm encounters difficulties in establishing a clear and distinct decision boundary for background differentiation.
- Further, as we focus on skeleton-based temporal action localization, extending the application of the action flow field to vision-based or hybrid tasks remains a substantial challenge.
- Finally, the scarcity of action-specific skeleton-based datasets limits broader applications of our framework.

References

- Alwassel, H., Giancola, S., and Ghanem, B. Tsp: Temporally-sensitive pretraining of video encoders for localization tasks. In *Proceedings of the IEEE/CVF International Conference on Computer Vision*, pp. 3173–3183, 2021.
- Buch, S., Escorcia, V., Shen, C., Ghanem, B., and Carlos Niebles, J. Sst: Single-stream temporal action proposals. In *Proceedings of the IEEE conference on Computer Vision and Pattern Recognition*, pp. 2911–2920, 2017.
- Caron, M., Misra, I., Mairal, J., Goyal, P., Bojanowski, P., and Joulin, A. Unsupervised learning of visual features by contrasting cluster assignments. *Advances in neural information processing systems*, 33:9912–9924, 2020.
- Carreira, J. and Zisserman, A. Quo vadis, action recognition? a new model and the kinetics dataset. In *proceedings of the IEEE Conference on Computer Vision and Pattern Recognition*, pp. 6299–6308, 2017.
- Chen, T., Kornblith, S., Norouzi, M., and Hinton, G. A simple framework for contrastive learning of visual representations, 2020a. URL <http://arxiv.org/abs/2002.05709>. cite arxiv:2002.05709Comment: ICML’2020. Code and pretrained models at <https://github.com/google-research/simclr>.
- Chen, X. and He, K. Exploring simple siamese representation learning, 2020. URL <http://arxiv.org/abs/2011.10566>. cite arxiv:2011.10566Comment: Technical report, 10 pages.
- Chen, X., Fan, H., Girshick, R., and He, K. Improved baselines with momentum contrastive learning, 2020b. URL <http://arxiv.org/abs/2003.04297>. cite arxiv:2003.04297Comment: Tech report, 2 pages + references.
- Dollár, P., Rabaud, V., Cottrell, G., and Belongie, S. Behavior recognition via sparse spatio-temporal features. In *2005 IEEE international workshop on visual surveillance and performance evaluation of tracking and surveillance*, pp. 65–72. IEEE, 2005.
- Du, Y., Wang, W., and Wang, L. Hierarchical recurrent neural network for skeleton based action recognition. In *Proceedings of the IEEE conference on computer vision and pattern recognition*, pp. 1110–1118, 2015.
- Feichtenhofer, C., Fan, H., Malik, J., and He, K. Slowfast networks for video recognition. In *Proceedings of the IEEE/CVF international conference on computer vision*, pp. 6202–6211, 2019.
- Grill, J.-B., Strub, F., Altché, F., Tallec, C., Richemond, P., Buchatskaya, E., Doersch, C., Avila Pires, B., Guo, Z., Gheshlaghi Azar, M., Piot, B., kavukcuoglu, k., Munos, R., and Valko, M. Bootstrap your own latent - a new approach to self-supervised learning. In *Advances in Neural Information Processing Systems*, volume 33, pp. 21271–21284. Curran Associates, Inc., 2020. URL https://proceedings.neurips.cc/paper_files/paper/2020/file/f3ada80d5c4ee70142b17b8192b2958e-Paper.pdf.
- Guo, T., Liu, H., Chen, Z., Liu, M., Wang, T., and Ding, R. Contrastive learning from extremely augmented skeleton sequences for self-supervised action recognition. In *Proceedings of the AAAI Conference on Artificial Intelligence*, volume 36, pp. 762–770, 2022.
- He, K., Zhang, X., Ren, S., and Sun, J. Deep residual learning for image recognition. In *Proceedings of the IEEE conference on computer vision and pattern recognition*, pp. 770–778, 2016.
- He, K., Fan, H., Wu, Y., Xie, S., and Girshick, R. Momentum contrast for unsupervised visual representation learning. In *Proceedings of the IEEE/CVF conference on computer vision and pattern recognition*, pp. 9729–9738, 2020.
- Heilbron, F. C., Niebles, J. C., and Ghanem, B. Fast temporal activity proposals for efficient detection of human actions in untrimmed videos. In *Proceedings of the IEEE conference on computer vision and pattern recognition*, pp. 1914–1923, 2016.
- Huang, L., Wang, L., and Li, H. Foreground-action consistency network for weakly supervised temporal action localization. In *Proceedings of the IEEE/CVF international conference on computer vision*, pp. 8002–8011, 2021.
- Jiang, B., Chen, X., Liu, W., Yu, J., Yu, G., and Chen, T. Motiongpt: Human motion as a foreign language. *arXiv preprint arXiv:2306.14795*, 2023.
- Ke, Q., Bennamoun, M., An, S., Sohel, F., and Boussaid, F. A new representation of skeleton sequences for 3d action recognition. In *Proceedings of the IEEE conference on computer vision and pattern recognition*, pp. 3288–3297, 2017.
- Lee, D., Kim, C., Kim, S., Cho, M., and Han, W.-S. Autoregressive image generation using residual quantization. In *Proceedings of the IEEE/CVF Conference on Computer Vision and Pattern Recognition*, pp. 11523–11532, 2022.

- Lin, J., Gan, C., and Han, S. Tsm: Temporal shift module for efficient video understanding. In *Proceedings of the IEEE/CVF international conference on computer vision*, pp. 7083–7093, 2019a.
- Lin, L., Zhang, J., and Liu, J. Actionlet-dependent contrastive learning for unsupervised skeleton-based action recognition. In *Proceedings of the IEEE/CVF Conference on Computer Vision and Pattern Recognition*, pp. 2363–2372, 2023.
- Lin, T., Zhao, X., and Shou, Z. Temporal convolution based action proposal: Submission to activitynet 2017. *arXiv preprint arXiv:1707.06750*, 2017.
- Lin, T., Liu, X., Li, X., Ding, E., and Wen, S. Bmn: Boundary-matching network for temporal action proposal generation. In *Proceedings of the IEEE/CVF international conference on computer vision*, pp. 3889–3898, 2019b.
- Liu, J., Shahroudy, A., Xu, D., and Wang, G. Spatio-temporal lstm with trust gates for 3d human action recognition. In *Computer Vision–ECCV 2016: 14th European Conference, Amsterdam, The Netherlands, October 11–14, 2016, Proceedings, Part III 14*, pp. 816–833. Springer, 2016.
- Liu, M., Liu, H., and Chen, C. Enhanced skeleton visualization for view invariant human action recognition. *Pattern Recognition*, 68:346–362, 2017.
- Mahmood, N., Ghorbani, N., Troje, N. F., Pons-Moll, G., and Black, M. J. Amass: Archive of motion capture as surface shapes. In *Proceedings of the IEEE/CVF international conference on computer vision*, pp. 5442–5451, 2019.
- Noguchi, C. and Tanizawa, T. Ego-vehicle action recognition based on semi-supervised contrastive learning. In *Proceedings of the IEEE/CVF Winter Conference on Applications of Computer Vision (WACV)*, pp. 5988–5998, January 2023.
- Pan, J., Chen, S., Shou, M. Z., Liu, Y., Shao, J., and Li, H. Actor-context-actor relation network for spatio-temporal action localization. In *Proceedings of the IEEE/CVF Conference on Computer Vision and Pattern Recognition*, pp. 464–474, 2021.
- Punnakkal, A. R., Chandrasekaran, A., Athanasiou, N., Quiros-Ramirez, A., and Black, M. J. Babel: Bodies, action and behavior with english labels. In *Proceedings of the IEEE/CVF Conference on Computer Vision and Pattern Recognition*, pp. 722–731, 2021.
- Qian, R., Meng, T., Gong, B., Yang, M.-H., Wang, H., Belongie, S., and Cui, Y. Spatiotemporal contrastive video representation learning. In *Proceedings of the IEEE/CVF Conference on Computer Vision and Pattern Recognition*, pp. 6964–6974, 2021.
- Rajasegaran, J., Pavlakos, G., Kanazawa, A., Feichtenhofer, C., and Malik, J. On the benefits of 3d pose and tracking for human action recognition. In *Proceedings of the IEEE/CVF Conference on Computer Vision and Pattern Recognition*, pp. 640–649, 2023.
- Sarto, S., Barraco, M., Cornia, M., Baraldi, L., and Cucchiara, R. Positive-augmented contrastive learning for image and video captioning evaluation. In *Proceedings of the IEEE/CVF Conference on Computer Vision and Pattern Recognition (CVPR)*, pp. 6914–6924, June 2023.
- Shi, L., Zhang, Y., Cheng, J., and Lu, H. Two-stream adaptive graph convolutional networks for skeleton-based action recognition. In *Proceedings of the IEEE/CVF conference on computer vision and pattern recognition*, pp. 12026–12035, 2019.
- Taylor, G. W., Fergus, R., LeCun, Y., and Bregler, C. Convolutional learning of spatio-temporal features. In *Computer Vision–ECCV 2010: 11th European Conference on Computer Vision, Heraklion, Crete, Greece, September 5–11, 2010, Proceedings, Part VI 11*, pp. 140–153. Springer, 2010.
- Tran, D., Bourdev, L., Fergus, R., Torresani, L., and Paluri, M. Learning spatiotemporal features with 3d convolutional networks. In *Proceedings of the IEEE international conference on computer vision*, pp. 4489–4497, 2015.
- Tu, Z., Li, H., Zhang, D., Dauwels, J., Li, B., and Yuan, J. Action-stage emphasized spatiotemporal vlad for video action recognition. *IEEE Transactions on Image Processing*, 28(6):2799–2812, 2019.
- Van Den Oord, A., Vinyals, O., et al. Neural discrete representation learning. *Advances in neural information processing systems*, 30, 2017.
- Vemulapalli, R., Arrate, F., and Chellappa, R. Human action recognition by representing 3d skeletons as points in a lie group. In *Proceedings of the IEEE conference on computer vision and pattern recognition*, pp. 588–595, 2014.
- Wang, H. and Schmid, C. Action recognition with improved trajectories. In *Proceedings of the IEEE international conference on computer vision*, pp. 3551–3558, 2013.
- Wang, J., Jiao, J., and Liu, Y.-H. Self-supervised video representation learning by pace prediction. In *Computer Vision–ECCV 2020: 16th European Conference, Glasgow*,

- UK, August 23–28, 2020, *Proceedings, Part XVII 16*, pp. 504–521. Springer, 2020.
- Wang, L., Xiong, Y., Wang, Z., Qiao, Y., Lin, D., Tang, X., and Van Gool, L. Temporal segment networks: Towards good practices for deep action recognition. In *European conference on computer vision*, pp. 20–36. Springer, 2016.
- Wang, X. and Gupta, A. Videos as space-time region graphs. In *Proceedings of the European conference on computer vision (ECCV)*, pp. 399–417, 2018.
- Wang, X., Girshick, R., Gupta, A., and He, K. Non-local neural networks. In *Proceedings of the IEEE conference on computer vision and pattern recognition*, pp. 7794–7803, 2018.
- Wu, Z., Xiong, Y., Yu, S. X., and Lin, D. Unsupervised feature learning via non-parametric instance discrimination. In *Proceedings of the IEEE Conference on Computer Vision and Pattern Recognition (CVPR)*, June 2018.
- Xu, H., Das, A., and Saenko, K. R-c3d: Region convolutional 3d network for temporal activity detection. In *Proceedings of the IEEE international conference on computer vision*, pp. 5783–5792, 2017.
- Xu, M., Zhao, C., Rojas, D. S., Thabet, A., and Ghanem, B. G-tad: Sub-graph localization for temporal action detection. In *Proceedings of the IEEE/CVF conference on computer vision and pattern recognition*, pp. 10156–10165, 2020.
- Xu, M., Pérez-Rúa, J.-M., Escorcia, V., Martinez, B., Zhu, X., Zhang, L., Ghanem, B., and Xiang, T. Boundary-sensitive pre-training for temporal localization in videos. In *Proceedings of the IEEE/CVF International Conference on Computer Vision*, pp. 7220–7230, 2021a.
- Xu, M., Perez-Rua, J.-M., Zhu, X., Ghanem, B., and Martinez, B. Low-fidelity end-to-end video encoder pre-training for temporal action localization. *arXiv preprint arXiv:2103.15233*, 2021b.
- Yan, S., Xiong, Y., and Lin, D. Spatial temporal graph convolutional networks for skeleton-based action recognition. In *Proceedings of the AAAI conference on artificial intelligence*, volume 32, 2018.
- Yang, C., Xu, Y., Dai, B., and Zhou, B. Video representation learning with visual tempo consistency. *arXiv preprint arXiv:2006.15489*, 2020.
- Yao, H., Song, Z., Zhou, Y., Ao, T., Chen, B., and Liu, L. Moconvq: Unified physics-based motion control via scalable discrete representations. *arXiv preprint arXiv:2310.10198*, 2023.
- Yu, Q. and Fujiwara, K. Frame-level label refinement for skeleton-based weakly-supervised action recognition. In *Proceedings of the AAAI Conference on Artificial Intelligence*, volume 37, pp. 3322–3330, 2023.
- Zeghidour, N., Luebs, A., Omran, A., Skoglund, J., and Tagliasacchi, M. Soundstream: An end-to-end neural audio codec. *IEEE/ACM Transactions on Audio, Speech, and Language Processing*, 30:495–507, 2021.
- Zhang, C., Cao, M., Yang, D., Chen, J., and Zou, Y. Cola: Weakly-supervised temporal action localization with snippet contrastive learning. In *Proceedings of the IEEE/CVF Conference on Computer Vision and Pattern Recognition*, pp. 16010–16019, 2021.
- Zhang, C., Yang, T., Weng, J., Cao, M., Wang, J., and Zou, Y. Unsupervised pre-training for temporal action localization tasks. In *Proceedings of the IEEE/CVF Conference on Computer Vision and Pattern Recognition*, pp. 14031–14041, 2022.
- Zhang, J., Zhang, Y., Cun, X., Huang, S., Zhang, Y., Zhao, H., Lu, H., and Shen, X. T2m-gpt: Generating human motion from textual descriptions with discrete representations. *arXiv preprint arXiv:2301.06052*, 2023.

A. Implementation Details

We apply a two-codebook Residual VQ-VAE structure for the segmentation and *pre-action* segmentation. The first codebook c^{VQ} is set for VQ layer, while its quantization results are considered as the *pre-action class*. The second codebook c^{RVQ} is shared by all the RVQ layers, which is only used for the action flow field decoders \mathcal{U} and \mathcal{B} . In most of our experiments, we utilize 4 RVQ layers, and the code numbers of c^{VQ} and c^{RVQ} are 64 and 256, respectively. The codebooks are updated by exponential moving averages (EMA).

Besides, to improve the usage of these codebooks, and avoid the discrete latent code Z is the same as continuous feature F , we reduce the dimensionality of F to 16 through a linear layer before performing quantization. After quantization, we will use another linear layer to increase its dimensionality back to 256. We calculate the commitment loss based on the features after dimensionality reduction.

We present the pseudo code of the training process of BID in Algorithm 1.

B. More quantitative analysis

Table 5. Numerical results on the different number of pre-action classes.

Subset-Union						
Method	Detection mAP @ IoU (%)					Avg
	0.1	0.2	0.3	0.4	0.5	
$K = 16$	41.80	38.52	34.17	28.89	23.12	33.30
$K = 32$	42.31	38.14	<u>34.28</u>	<u>29.23</u>	23.00	<u>33.39</u>
$K = 64$	<u>42.09</u>	<u>38.23</u>	34.58	30.27	24.15	33.86
$K = 128$	41.57	37.08	33.33	28.74	<u>23.01</u>	32.74
$K = 256$	39.81	35.62	32.15	27.36	22.20	31.43

We evaluate the influence of the number of *pre-action classes* in the VQ layers on the union subset of the three subsets we used in Section 5 with 12 action classes. An interesting observation is that despite the union set requiring the detection of 12 actions, as opposed to just 4 in individual subsets, our choice of K remained consistent in yielding similar conclusions. $K = 64$ is still the best choice for the experiments. The reason is that an optimal choice of K enables better-distinguishing action segments during pre-training, a distinction that universally benefits downstream tasks.

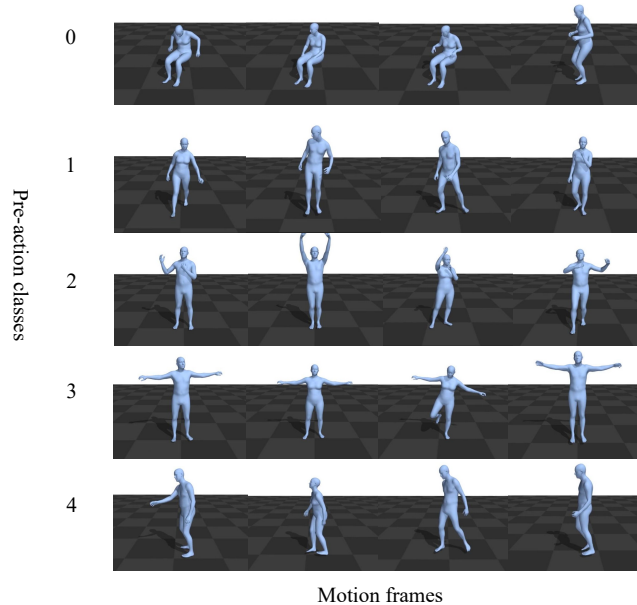


Figure 4. Visualization for pre-action classes and their corresponding motion frames.

C. Visual results

C.1. Visualization for Pre-action Classes

In Figure 4, we present some *pre-action classes* learned by our unsupervised pre-training method with their corresponding motion frames. We can observe that these *pre-action classes* are related to specific human body movements, such as sitting, arm lifting, and T-pose. Through these *pre-action classes*, our pre-training model can segment input motion sequences into meaningful segments. Through the fine-tuning process, this ability of segmentation and classification are transferred to the domain of human annotation.

C.2. Visual Results for Pre-Training

In Figure 5, we compare some *pre-action segmentation* predicted by our unsupervised pre-training model with the corresponding ground-truth segment, where different colors represent different *pre-action classes* or ground-truth labels. We observe that, despite the absence of ground truth supervision during the pre-training process, our model still achieves segmentation results quite close to the ground truth. Furthermore, our pre-training process is capable of learning action patterns not annotated in the ground truth labels, such as the repetitive bending and raising of hands by the character in sequence (a). Besides, we include a video for visualizing the pre-training results, further demonstrating the information learned by our algorithm.

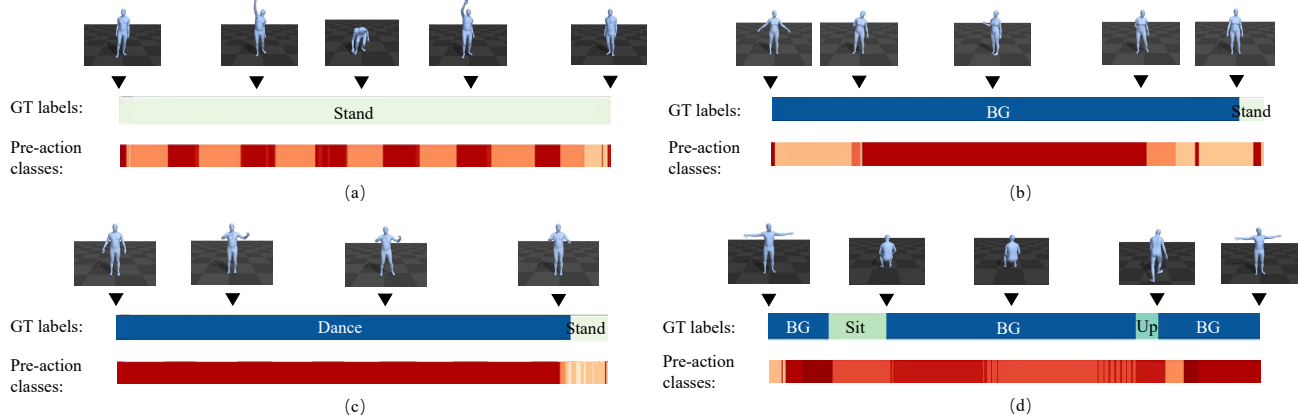


Figure 5. Visualization for discrete encode results of pre-training model

C.3. Visualization for Fine-Tuning Process

To enable fine-tuning process, we add a linear classifier after the encoder E . We want to understand the changes in features during the fine-tuning process. Thus, we utilize freeze pre-trained VQ layer and codebook c^{VQ} to quantize the features outputted during the fine-tuning process.

We present some samples in Figure 6. In our initial guess, the finetuning process mainly involved the update of features and the aggregation of adjacent segments. Sequence (a) aligns with our original guess. However, we found that this pattern does not apply to all sequences. For instance, in sequence (b), the pre-trained model attempts to predict two rough transition processes (red segments) for sit state. As fine-tuning progresses, these transitions are not absorbed into the 'sit' or 'stand up' but become more precise, even though the ground truth does not provide information about the transitions. In sequence (c), we further discovered that even though our network could roughly segregate the background of an action during pre-training, it is still capable of further dissecting the background through the finetuning process. We believe this indicates that our pre-training process has learned a representation that can effectively express different action classes, which can be refined through a labeled fine-tuning process, resulting in accurate and fine-grained action representations.

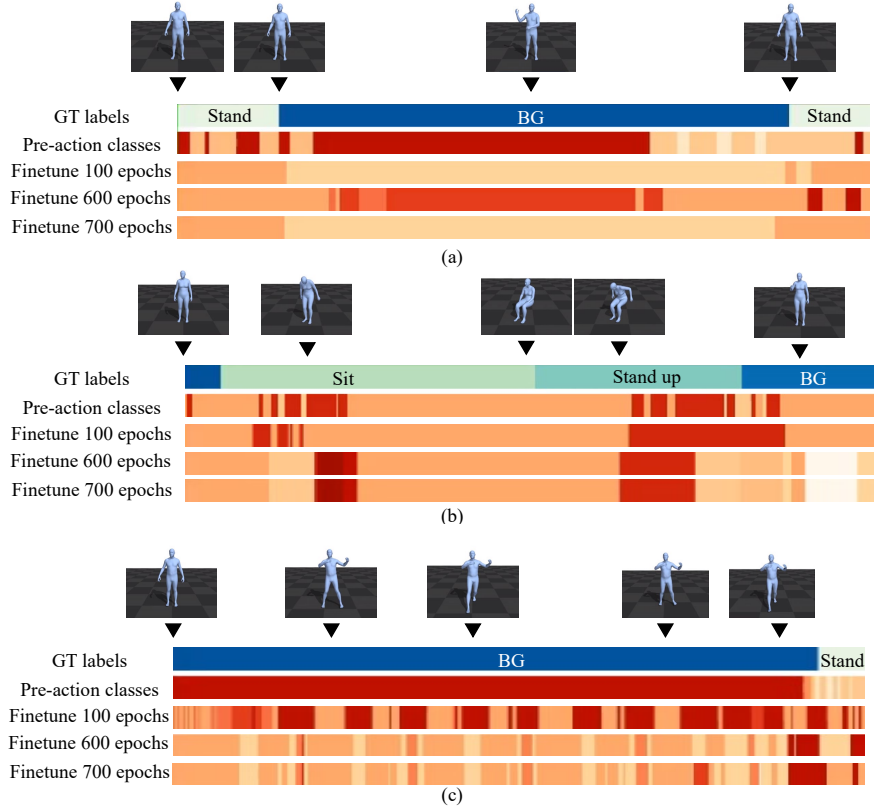


Figure 6. Visualization of discrete encode results for finetuning model

D. Statistical analysis

We learn a discrete encoder to segment the input motion sequences and classify the segments as pre-action classes. Although these pre-action classes are not equivalent to annotated action classes, we still hope there is a correlation between them. We present the confusion map for pre-action classes and ground truth labels, where we set $K = 16$, in figure 7. We found that some pre-action classes have a stronger association with a few specific action labels, like pre-action 12 is highly related to action sit and stand up. Some pre-action classes have connections with multiple different actions, like pre-actions 1 and 2.

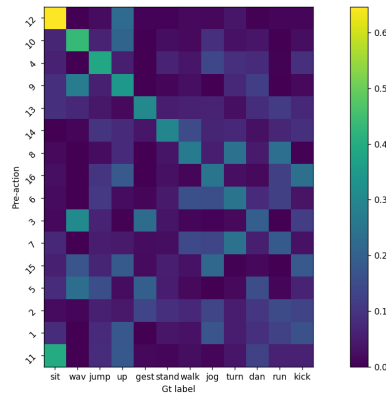


Figure 7. Confusion map for pre-action classes and ground truth action classes.

Algorithm 1 The training process of BID

- 1: **Input:** Skeleton-based motion sequence $S = s_i \in \mathbb{R}^{T \times D}$, boundary loss weight λ^{bound} and commitment loss weight λ^{com} .
 - 2: **Initialization:** Linear encoder E , VQ layer VQ , RVQ layers $RVQ^l_{l=0}$, Interior decoder \mathcal{U} and Boundary decoder \mathcal{B} .
 - 3: $F \leftarrow E(S)$ (Equation 3)
 - 4: $Z^0 \leftarrow VQ(F)$
 - 5: Segment S into $\{p_m\}_{m=0}^M$ based on Z^0
 - 6: Copy end frames of $\{p_m\}_{m=0}^M$ to get S^e
 - 7: $l \leftarrow 1$
 - 8: **while** $l \leq L$ **do**
 - 9: $r^l \leftarrow F - Z^0 - \sum_{j=0}^{L-1} R^j$
 - 10: $R^l \leftarrow RVQ^l(r^l)$
 - 11: **end while**
 - 12: $Z = Z^0 + \sum_{j=1}^L R^j$ (Equation 6)
 - 13: $\mathcal{L}^{com} \leftarrow \|F - Z\|_2^2$ (Equation 5)
 - 14: Apply EMA update to the codebook of VQ and RVQ
 - 15: Generate random mask $M \in \mathbb{R}^T$
 - 16: $S' \leftarrow \mathcal{U}(F \circ M, Z)$
 - 17: $\mathcal{L}^{in} \leftarrow \|S - S'\|_2^2$ (Equation 7)
 - 18: $S^{e'} \leftarrow \mathcal{B}(F, Z)$
 - 19: $\mathcal{L}^{bound} \leftarrow \|S^e - S^{e'}\|_2^2$ (Equation 8)
 - 20: $L^{total} \leftarrow \mathcal{L}^{in} + \lambda^{bound} \mathcal{L}^{bound} + \lambda^{com} \mathcal{L}^{com}$ (Equation 9)
-

E. Architecture of Our Network

We utilize TCN-based structures for both encoder and decoders, which extracts spatio features for human motion through convolution with a kernel size of 1, and extract temporal features through dilation convolution and larger kernels (9 or 3). We list the details of our network architecture in Table 6. The decoders \mathcal{U} and \mathcal{B} share the same architecture.

F. Symbol meaning

We list the symbols we used in the paper and their meaning in Table 7.

G. More visualization

We show more visualization in Figure 8

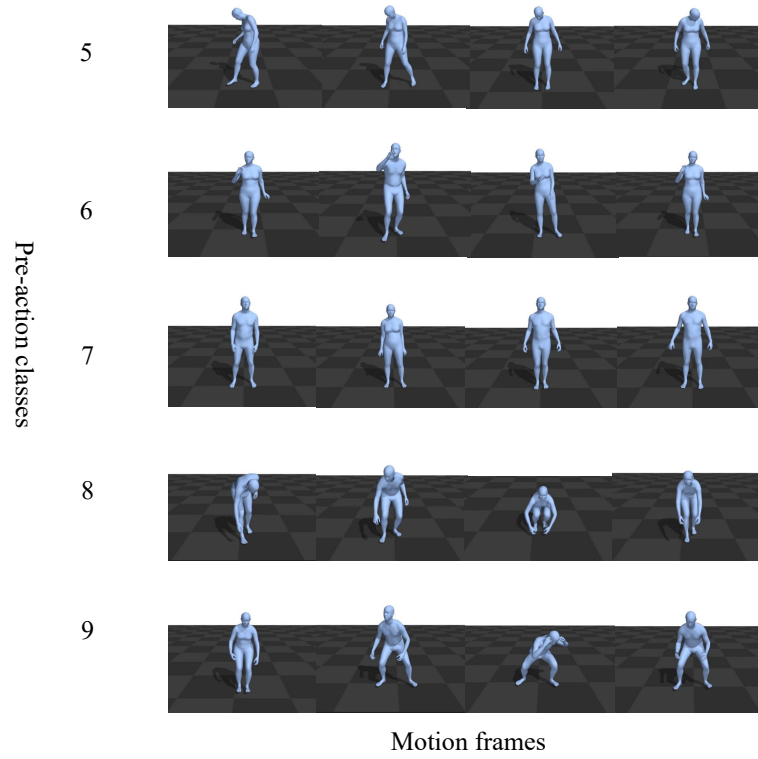


Figure 8. More visualization for pre-action classes and their corresponding motion frames.

Table 6. Architecture of our Method

Components	Architecture
Linear Encoder	(0): Conv1D(J*3, 256, kernel_size=(3,), stride=(1,), padding=(1,))
	(1): ReLU()
	(2): $2 \times$ Sequential((0): Conv1d(256, 256, kernel_size=(3,), stride=(1,), padding=(1,)) (1): ResConv1DBlock((0): (activation1): ReLU() (1): (conv1): Conv1D(256, 256, kernel_size=(3,), stride=(1,), padding=(9,), dilation=(9,)) (2): (activation2): ReLU() (3): (conv2): Conv1D(256, 256, kernel_size=(1,), stride=(1,))) (2): ResConv1DBlock((0): (activation1): ReLU() (1): (conv1): Conv1D(256, 256, kernel_size=(3,), stride=(1,), padding=(3,), dilation=(3,)) (2): (activation2): ReLU() (3): (conv2): Conv1D(256, 256, kernel_size=(1,), stride=(1,))) (3): ResConv1DBlock((0): (activation1): ReLU() (1): (conv1): Conv1D(256, 256, kernel_size=(3,), stride=(1,), padding=(1,)) (2): (activation2): ReLU() (3): (conv2): Conv1D(256, 256, kernel_size=(1,), stride=(1,)))
Residual VQ	(0): (conv1): Conv1D(256, 16, kernel_size=(1,), stride=(1,)) (1): (codebook_class): nn.Parameter((64, 16), requires_grad=False) (2): (codebook_residual): nn.Parameter((64, 16), requires_grad=False) (3): (conv2): Conv1d: Conv1D(16, 256, kernel_size=(1,), stride=(1,))
Decoder	(0): $2 \times$ Sequential((0): Conv1d(256, 256, kernel_size=(3,), stride=(1,), padding=(1,)) (1): ResConv1DBlock((0): (activation1): ReLU() (1): (conv1): Conv1D(256, 256, kernel_size=(3,), stride=(1,), padding=(9,), dilation=(9,)) (2): (activation2): ReLU() (3): (conv2): Conv1D(256, 256, kernel_size=(1,), stride=(1,))) (2): ResConv1DBlock((0): (activation1): ReLU() (1): (conv1): Conv1D(256, 256, kernel_size=(3,), stride=(1,), padding=(3,), dilation=(3,)) (2): (activation2): ReLU() (3): (conv2): Conv1D(256, 256, kernel_size=(1,), stride=(1,))) (3): ResConv1DBlock((0): (activation1): ReLU() (1): (conv1): Conv1D(256, 256, kernel_size=(3,), stride=(1,), padding=(1,)) (2): (activation2): ReLU() (3): (conv2): Conv1D(256, 256, kernel_size=(1,), stride=(1,))) (2) Conv1D(256, 256, kernel_size=(1,), stride=(1,)) (1): ReLU() (2): Conv1D(256, 75, kernel_size=(1,), stride=(1,))

Table 7. The meaning of symbols.

Symbol	Meaning
\mathcal{S}	Skeleton-based motion sequence dataset
S	Skeleton-based motion sequence
s_i	i -th frame in sequence S
T	Number of frames in sequence S
J	Number of freedom of skeleton joints
N	Pre-defined number of pre-action class
M	Number of {pre-action} segments in sequence S
p	<i>Pre-action</i> segment
p^m	m -th <i>pre-action</i> segment in sequence S
t_m^b	The begging timestamp of p_m
t_m^e	The ending timestamp of p_m
a_m	The <i>pre-action</i> class of p_m
\mathcal{G}	Flow field function
t	Timestamp
x_t	object’s position at time t .
\mathcal{G}^{a_m}	Flow field function related to <i>pre-action</i> class a_m
\mathcal{E}	Motion encoding function
E	Linear motion encoder
F	Sequence feature (the output of E)
f_i	i -th pre-frame feature of F_i (the continuous feature of s_i)
c	Codebook
Z	Discrete latent code projected from F
VQ	VQ layer
c_j	j -th discrete latent in c
sg	Stop gradient
\mathcal{L}^{com}	Commitment loss
RVQ	Residual VQ layer
Z^0	Discrete latent code projected from F by VQ layer
L	Number of RVQ layers
R^l	Residual discrete latent code projected from $F - Z^0 - \sum_{j=1}^{j < l-1} R^j$ by l -th RVQ layer
c^{VQ}	Codebook of VQ layer
c^{RVQ}	Shared codebook of RVQ layers
M	Random mask
\mathcal{U}	Interior decoder
\mathcal{L}^{in}	Interior loss
\mathcal{B}	Boundary decoder
$P(i)$	The boundary frame timestamp t_m^e of predicted <i>pre-action</i> segment p_m tht contains frame s_i
S^e	End-of-segment sequence $\{s_{P(i)}\}_{i=1}^T$
\mathcal{L}^{bound}	Boundary loss
\mathcal{L}^{total}	Total loss
λ^{bound}	Loss weight for \mathcal{L}^{bound}
λ^{com}	Loss weight for \mathcal{L}^{com}